



## Effect of Source-to-site Distance on Spatial variation of Ground Motions

Rui-fang Yu<sup>(1)</sup>, Abduwaris Abduwahit<sup>(2)</sup>, Yan-xiang Yu<sup>(3)</sup>

<sup>(1)</sup> *Institute of Geophysics, China Earthquake Administration, Beijing, China, yrfang126@126.com*

<sup>(2)</sup> *Earthquake Administration of Xinjiang Uygur Autonomous Region, Wulumuqi, China, waris2t@163.com*

<sup>(3)</sup> *Institute of Geophysics, China Earthquake Administration, Beijing, China, yuyx@cea-igp.ac.cn*

### **Abstract**

Recordings from dense seismograph arrays are widely used to study spatial variations of ground motion. In this study, the authors devote to discuss the spatial variation of ground motion based on the recordings observed from dense arrays, especially to analyze the effect of source-to-site distance on spatial variation of ground motion. The recordings been employed in this study include 2008 Wenchuan earthquake (M 8.0) from Zigong Seismograph Array in China, 2003 San Simeon earthquake (M 6.5) and 2004 Parkfield earthquake (M 6.0) from UPSAR, all of which are of great value in studying the spatial variations of seismic ground motion at engineering scales, especially the spatial variations of large far-field and near-field earthquakes. Firstly, authors calculated and simulated the coherency functions through application of digital signal processing technology based on the accelerograms coming from different earthquake. Then, the variation mechanisms of the coherency functions at various directions along with the separation distance and frequency changes were analyzed. The results showed that source-to-site distance affects the variation rate of lagged coherency function along with separation distances in both low-frequency and high-frequency ranges. Therefore, we define “coherency cut-off frequency” to distinguish different variation rates of the lagged coherency function along with separation distances in both low-frequency and high-frequency ranges. And three earthquakes with different source-to-site distance were compared to determine the values of coherency cut-off frequency. Based on these, a new piecewise model was established to simulate the variation of lagged coherency function, including parameters suitable for the conditions of earthquake in the near and far fields. This model relates to the coherency cut-off frequency and better reflects the changes of the lagged coherency function along with the frequency and separation distance changes. In conclusion, the model established in this study provides an effective method of simulating the spatial correlations of ground motions at local sites with known source-to-site distances.

*Keywords: spatial variation; coherency function; Wenchuan earthquake; San Simeon earthquake; Parkfield earthquake*



## 1. Introduction

Spatial variation of seismic ground motions denotes the differences in amplitude and phase of seismic motions recorded over extended areas, which exerts important effect on the response of lifelines such as bridges and pipelines. Because these structures extend over long distances parallel to the ground, their supports undergo different motions during an earthquake, which can increase the response of extended structures beyond the response expected provided that the input motions at the structures' supports were assumed to be identical<sup>[1-3]</sup>. At present, ground motion spatial variation has been extensively studied based on the dense seismograph array data, in which some factors, such as the wave passage effect, source, propagation path and site conditions, irregular topography and random soil properties were considered<sup>[4,5]</sup>. Many models of coherency function have been proposed to describe the spatial variation of ground motion<sup>[6-9]</sup>, and these models have been widely used to simulate spatially varying ground motions to calculate the dynamic responses of large-span structures under multi-supported earthquake input<sup>[10-14]</sup>. However, these coherency models do not completely meet engineering needs, especially the effect of some factors on spatial variation, such as neighboring topography, local site condition, and source-to-site distance. Therefore, fresh and detailed data from an especially large earthquake for a more accurate analysis of spatial variation in earthquake motion is needed.

The aim of this study is to analyze the source-to-site distance effect on spatial variation of ground motion. For this destiny, strong ground motions observed from dense arrays were intendedly selected, including 2008 Wenchuan earthquake (M 8.0) from Zigong Seismograph Array (ZGSA) in China, 2003 San Simeon earthquake (M 6.5) and 2004 Parkfield earthquake (M 6.0) from the U.S. Geological Survey Parkfield Dense Seismograph Array (UPSAR). Firstly, we calculated and simulated the coherency functions through application of digital signal processing technology based on the accelerograms coming from different earthquake. Then, the variation mechanisms of the coherency functions at various directions along with the separation distance and frequency changes were analyzed. The results showed that source-to-site distance affects variation rate of lagged coherency function along with separation distances in both low-frequency and high-frequency ranges. Therefore, we define "coherency cut-off frequency" to distinguish different variation rates of the lagged coherency function along with separation distances in both low-frequency and high-frequency ranges. And three earthquakes with different source-to-site distance were compared to determine the values of coherency cut-off frequency. Finally, a new piecewise model was established to simulate the variation of lagged coherency function, including parameters suitable for the conditions of earthquake in the near and far fields. This model relates to the coherency cut-off frequency and better reflects the changes of the lagged coherency function along with the frequency and separation distance changes. Though well supported by the data, many of our observations remain in part qualitative because of the complexity of the ground motions.

## 2. Data and Processing

The recordings of three earthquakes from two dense seismograph arrays were selected to analyze the effect of source-to-site distance on variation of ground motion. The first was the recordings from 2008 Wenchuan earthquake recorded by the Zigong Seismograph Array (ZGSA), which was installed in Sichuan Province, China in 2007. The ZGSA includes eight irregularly spaced seismograph stations as shown in Fig.1. Each station has three-component force-balance accelerometers (FBAs). Each channel is digitized at 18 bits and 200 samples per sec. These stations are spaced irregularly with inter-station spacing ranging from 47 m to about 385 m. There is a 72-m elevation difference between the lowest station (Z0 or Z1) and the highest station (Z6). Moreover, the distances from the Wenchuan event epicenter to each station about 226 km, so these data are of great value to study the spatial variations of a large earthquake in far-field. And then, the recordings of the San Simeon and Parkfield earthquakes recorded by UPSAR were selected. UPSAR includes 14 seismograph stations spaced irregularly over hilltops with inter-station spacing ranging from 25



m to about 960 m, as is shown in Fig.2<sup>[15]</sup>. The source-to-site distances of the two events are 55.6 km and 11.6 km, respectively. The details of the three earthquakes are listed in Table 1.

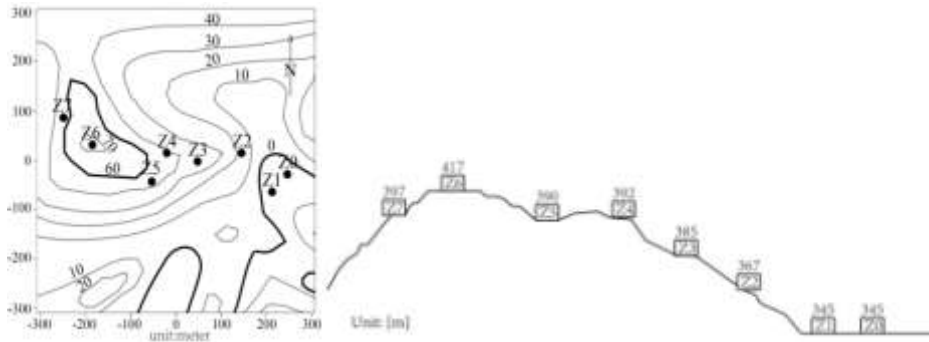


Fig. 1 – The locations of Zigong Seismograph Array (ZGSA)

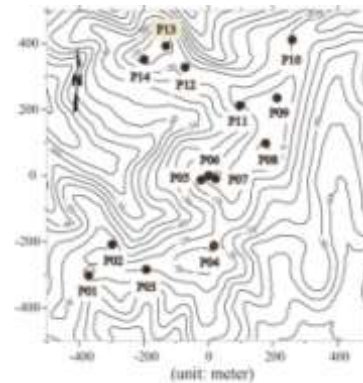


Fig. 2 – The locations of UPSAR

Table 1 – The details of three earthquakes

Event	Mag.	Source-to-site Dis.	Array	Station	Year
Wenchuan	8.0	226.3	Zigong	8	2008
San Simeon	6.5	55.6	UPSAR	14	2003
Parkfield	6.0	11.6	UPSAR	14	2004

Some studies on Taiwan and California earthquakes imply that most digital recordings are plagued by random baseline offsets, which is true for the ZGSA recordings used in this study as well. Ground motions for periods less than about 20 s are usually unaffected by specific baseline correction schemes<sup>[16-18]</sup>, so we applied a simple baseline correction scheme here: first, the mean of the entire record was removed from the whole record; then, an acausal fourth-order Butterworth low-cut filter with corner frequency of 0.05 Hz was applied to each record.

Seismic ground motions also incorporate random time delay fluctuations around the wave passage delay that are particular for each recording station. These arrival time perturbations are caused by the upward travel of the waves through horizontal variations of the geologic structure underneath the array<sup>[19]</sup>, and by deviations of the propagation pattern of the waves (recorded as arrival time) from that of plane wave propagation<sup>[20]</sup>. The wave passage effects control the complex exponential term of the coherency, and the



arrival time perturbations affect its absolute value, namely the lagged coherency. An approach that partially eliminates these effects from coherency estimates is the alignment of the data with respect to a reference station.

If the cross-covariance function of the motions between the two stations is defined as:

$$\hat{R}_{mn}(\tau) = \frac{1}{T} \int_0^{T-|\tau|} a_m(t) a_n(t+\tau) dt \quad |\tau| \leq T \quad (1)$$

where  $a_m(t)$  and  $a_n(t)$  are two time series in the same direction recordings. Let the duration of strong motion S-wave window be  $0 \leq t \leq T$ ,  $T = N\Delta t$ , with  $N$  being the number of samples in the recorded time series for window, and  $\Delta t$  the time step. It is iterated here that this window of the actual time history is assumed to be a segment of an infinite one with uniform characteristics through time (stationarity assumption). The cross covariance function is generally smoothed before it is further used as an estimator, and the smoothed cross covariance function is:

$$R_{mn}(\tau) = w(\tau) \hat{R}_{mn}(\tau) \quad (2)$$

where  $w(\tau)$  is the lag window, with properties  $w(\tau) = w(-\tau)$ ,  $w(\tau = 0) = 1$  and  $\int_{-\infty}^{\infty} w(\tau) = 1$ .

In this process, the cross correlation of the motions (the normalized cross covariance function of Eq. (2)) relative to the reference station is evaluated. The time corresponding to the highest correlation provides the delay in the arrival of the waves at the various stations relative to their arrival at the reference station. Once the motions are aligned, they become invariant to the reference station selection, but the value of the time delay required for alignment is relative, that is, it is affected by the choice of the reference station. For example, for ZGSA, the station Z1 located at the foot of hill is selected as the reference station. The arrival time perturbation related to reference station Z1 are eliminated by using Eq. (1). Then the cross correlation functions between station Z1 and other stations (Z0, Z4 and Z6) are calculated to illustrate the time perturbation alignment, as is shown in Fig.3. According to the time perturbation between two records, move the acceleration time series of station Z0, Z4 and Z6 forward or backward along the time axis, let the maximum value of cross correlation function of acceleration time series between station Z1 and other stations occur at the zero point in time axial, as is shown in Fig.4.

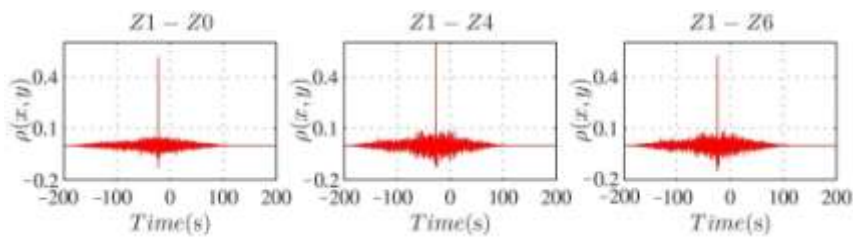


Fig. 3 – Correlation function before arrival time perturbation are modified

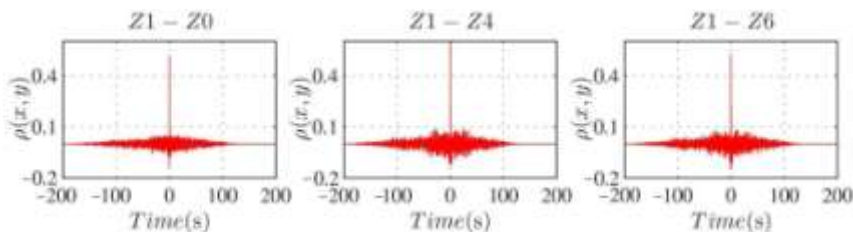


Fig. 4 – Correlation function after arrival time perturbation are modified



### 3. Lagged Coherency Function

For the stationary process, the cross spectral density (or cross spectrum) of the process is defined as the Fourier transform of the covariance function (Eq. (1)). The smoothed cross spectrum is evaluated by Fourier transforming (Eq. (2)):

$$S_{mn}(\omega) = \frac{1}{2\pi} \int_{-T}^T R_{mn}(\tau) e^{-i\omega\tau} d\tau \quad (3)$$

with  $i = \sqrt{-1}$  and  $\omega$  being the frequency (in rad/sec). Alternatively, the (smoothed) cross spectral estimates of the series can be evaluated directly in the frequency domain as follows:

$$S_{mn}(\omega_j) = \sum_{j=-M}^M W(j\Delta\omega) A_m^*(\omega_j + j\Delta\omega) A_n(\omega_j + j\Delta\omega) \quad (4)$$

where spectral window,  $W(\omega)$  is the Fourier transform of the lag window  $w(\tau)$ ,  $\Delta\omega$  is the frequency step, ( $\Delta\omega = 2\pi/T$ ),  $A_m(\omega)$  and  $A_n(\omega)$  are the scale discrete Fourier transform of the time histories  $a_m(t)$  and  $a_n(t)$ , respectively, and \* indicates complex conjugate.

Then the power spectral densities of motions (i.e.  $m \equiv n$  in Eq. (3) and (4)) are estimated from the analysis of data recorded at each station and are commonly referred to as point estimates of the motions:

$$S_{mm}(\omega_j) = \sum_{j=-M}^M W(j\Delta\omega) |A_m(\omega_j + j\Delta\omega)|^2 \quad (5)$$

It is obvious that the Fourier spectra of motions at various stations will not be identical. However, the assumption of spatial homogeneity in the random field implies that the power spectrum of motions is station independent. Then the coherency of seismic motions is obtained from the smoothed cross spectrum of motions between the two stations  $m$  and  $n$ , normalized with spectrum to corresponding power spectra as, e.g.<sup>[1,21]</sup>:

$$\gamma_{mn}(\omega, d) = \frac{S_{mn}(\omega, d)}{\sqrt{S_{mm}(\omega, d) S_{nn}(\omega, d)}} = |\gamma_{mn}(\omega, d)| \exp[i\theta(\omega, d)] \quad (6)$$

in which:  $S_{mn}(\omega, d)$  is the cross-power spectral density function of supports  $m$  and  $n$ ;  $S_{mm}(\omega, d)$  and  $S_{nn}(\omega, d)$  are the power spectral density functions of the supports  $m$  and  $n$ , respectively, which are the functions of frequency  $\omega$  and station-to-station distance  $d$ ;  $\exp[i\theta(\omega, d)]$  is used to describe the wave passage effect, i.e. the delay in the arrival of the waveforms at the more distant station caused by the propagation of waveforms. The expression  $|\gamma_{mn}(\omega, d)|$  is the lagged coherency, used to measure similarity in seismic motion, and varies from 0 to 1. In this study, we mainly discuss the variations of lagged coherency, because it is widely used in engineering practice to simulate multi-supported earthquake ground motion.

If it is considered that the smoothing widow is not used in the evaluation of the cross covariance function nor, alternatively, in the cross spectrum of series (Eq. (2) and (4)). Substitution of Eq. (4) and (5) into Eq. (6) yields the identity  $|\gamma_{mn}(\omega, d)| \equiv 1$  for any frequency  $\omega$  and station pair  $(m, n)$  regardless of the true coherency of the data. The information about the differences in the phases of the motions at the stations is introduced in the estimate through the smoothing process, which controls the statistical properties of the coherency as well as its resolution. It needs to be emphasized that coherency estimates depend strongly on the type of smoothing widow and the amounts of smoothing performed on the raw data. Abrahamson *et al.*<sup>[22]</sup> note that the choice of smoothing window should be directed not only from the statistical properties of the



coherency, but also from the purpose for that it is derived. In this study, an 11-point Hamming window is used to calculate the coherency function. It is evident that very good agreement can be obtained except for the frequencies near zero. In fact, theoretically, coherency should be unity as frequency tends to zero, however, coherency estimates from ground motion time histories, due to smoothing, can rarely reach this value. In this study, the lagged coherency  $|\gamma_{mn}(\omega, d)|$  is calculated to analyze the spatial variation of ground motion.

#### 4. Effect of Source-to-site Distance on Lagged Coherency Function

Suppose the interval of circular frequency is  $\Delta\omega = 0.1\pi$  and the considered frequency ranges from  $0.1\pi$  to  $20\pi$ , the variation of the lagged coherence function at each given frequency can be obtained. Fig.5 plots the variations of lagged coherency functions along with the separation distance  $d$  at 3 given frequencies ( $\omega = \pi, 3\pi, 10\pi$ ) for different directions, in which results calculated by Parkfield earthquake are marked by the symbol “o”, the values calculated by San Simeon event are marked by the symbol “\*”, and the values calculated by Wenchuan event are marked by the symbol “Δ”.

The results illustrate that the values calculated from near-field earthquakes decay faster than those from far-field earthquakes as the separation distances increase, in the low-frequency range. And in the high-frequency range, the values of far-field recording decay even more rapidly with increasing separation distance. Moreover, the variation rates of lagged coherency function along with separation distances in low-frequency range are quite different from that in high-frequency range, and for the different earthquake with different source-to-site distance, the frequencies distinguished to low and high frequencies are different from each other. For instance, for the Wenchuan earthquake, when  $\omega \leq 3\pi$ , the values are generally more than 0.8, especially in vertical direction, but when  $\omega > 3\pi$ , the degressive trend of the lagged coherency function with the separation distance elongation becomes significant. That is, there exists a “coherency cut-off frequency” (named as  $\omega_c$ ), before and after which, the variation of lagged coherency function is different.

In order to determine the value of corner frequency, we selected four models to simulate the lagged coherence functions of three earthquakes to find the variation of  $|\gamma_{mn}(\omega, d)|$  along with frequency and separation distance. The function forms of these models are expressed respectively as:

Model A <sup>[6]</sup>:

$$|\gamma(\omega, d)| = \exp[-(\rho_1\omega + \rho_2)d] \quad (7)$$

here  $\rho_1 = 2 \times 10^{-5} s/m$ ,  $\rho_2 = 8.8 \times 10^{-3} s/m$ .

Model B <sup>[9]</sup>:

$$|\gamma(\omega, d)| = A \exp\left(-\frac{2Bd}{av(\omega)}\right) + (1-A) \exp\left(-\frac{2Bd}{v(\omega)}\right) \quad (8)$$

here  $v(\omega) = k[1 + (\frac{\omega}{2\pi f_0})^b]^{-1/2}$ ,  $B = 1 - A + aA$ ,  $A = 0.736$ ,  $a = 0.147$ ,  $k = 5210m$ ,  $f_0 = 1.09Hz$ ,  $b = 2.78$ .

Model C <sup>[21]</sup>:

$$|\gamma(f, d)| = \exp[-(a + bf^2)d] \quad (9)$$

for the strike-slip fault,  $a = 1.3 \times 10^{-6}$ ,  $b = 2.38 \times 10^{-5}$  for horizontal components and  $a = 9.8 \times 10^{-6}$ ,  $b = 4.79 \times 10^{-5}$  for vertical direction.



Model  $D^{[23]}$ :

$$|\gamma(f, d)| = \exp(-\alpha fd) \quad (10)$$

where the value of  $\alpha$  varies  $(0.4-0.7) \times 10^{-3} \text{ sec}/m$ .

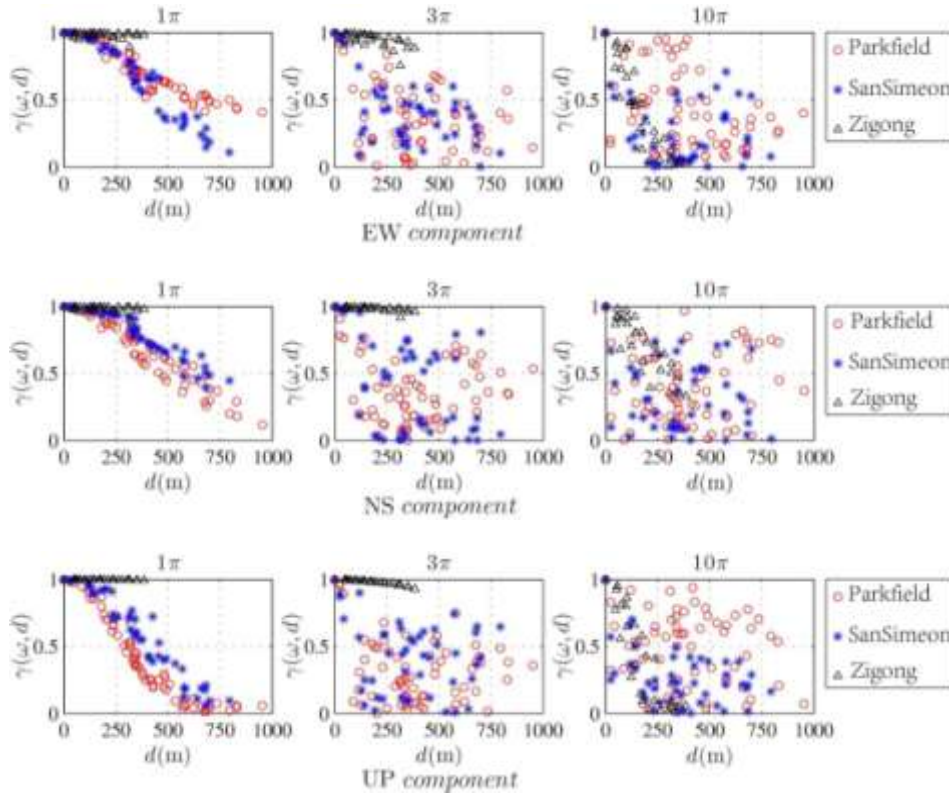
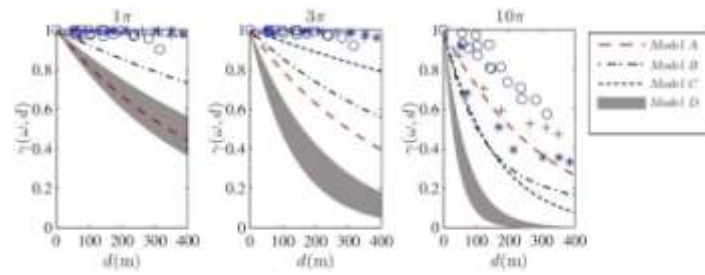


Fig. 5 – Plots showing the variation of lagged coherency functions of three earthquakes as a function of separation distances when  $\omega = \pi, 3\pi, 10\pi$

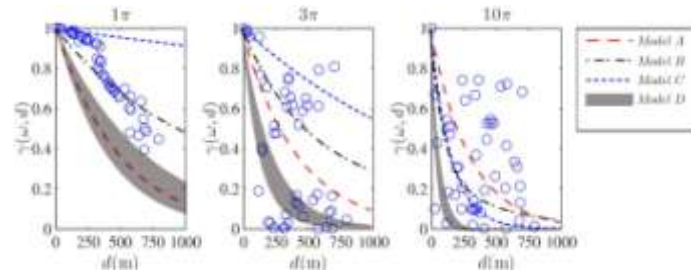
The fitting results of four models for NS components of three earthquakes at three frequencies ( $\omega = \pi, 3\pi, 10\pi$ ) are shown in Fig.6, in which gray band represents the variation of *Model D* because of its parameter range  $(0.4-0.7) \times 10^{-3} \text{ sec}/m$ . It is clear that fitting results of these models are affected by the frequency ranges. Table 2 lists the results of four models for three events in different frequency ranges, in which “S” represents satisfied fitting results, and “NS” represents the fitting results which are not satisfied with calculation data. It can be seen that *Model B* is satisfied with the calculation data of San Simeon earthquake, and *Model A* is satisfied with the calculation results of Parkfield earthquake. However, for the recordings of far-field earthquake, it seems that there are not suitable models to satisfy simultaneously the calculation results in the high-frequency and low-frequency ranges.

Table 2 – The comparison of fitting results for three earthquakes

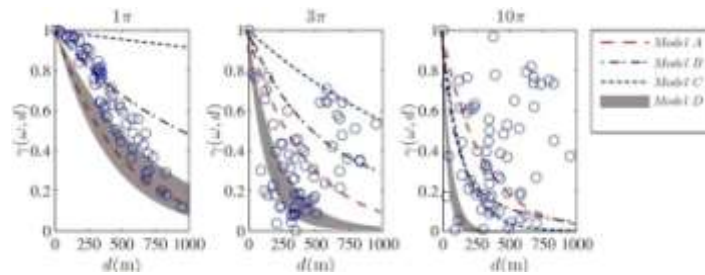
Events	Low-frequency range				High-frequency range			
	A	B	C	D	A	B	C	D
Wenchuan	NS	NS	S	NS	S	NS	NS	NS
San Simeon	NS	S	NS	NS	NS	S	S	S
Parkfield	S	NS	NS	S	S	S	S	NS



(a) Wenchuan earthquake



(b) San Simeon earthquake



(c) Parkfield earthquake

Fig. 6 – Fitting results of Models for NS components of three earthquakes when  $\omega = \pi, 3\pi, 10\pi$ 

Therefore, the variation rate of lagged coherency function along with separation distances for a series of given frequencies ( $\omega_i = \omega_{i-1} + 0.1\pi$ ) were calculated through simulation data corresponding frequency. The results denote that the corner frequency  $\omega_c$  relate to the source-to-site distance, which increase along with the increasing source-to-site distance. Table 3 listed the values of coherency cut-off frequency for three earthquakes.

In generally, when  $\omega \leq \omega_c$ , the degressive trend of the coherence function along with increasing station-to-station distance are obvious, but when  $\omega > \omega_c$ , the values become smaller gradually along with the separation distances prolonging and the discreteness of the data becomes larger with the increasing frequency. Furthermore, in the low-frequency ranges, the values calculated from near-field earthquakes decay faster than that from far-field earthquake along with the separation distances increasing. However, in the high-frequency ranges, the values of far-field recording decays even more rapidly with increasing separation distance.

Table 3 – The coherency cut-off frequency  $\omega_c$  of three earthquakes

Event	Wenchuan	San Simeon	Parkfield
Source-to-site Dis.	226.6km	55.6km	11.6km
$\omega_c$	$3\pi$	$1.5\pi$	$\pi$



## 5. Lagged Coherency Function Model of Earthquake Ground Motions

According to the above analysis, we conclude that satisfactory fitting results can be obtained if using different model parameters for different frequency ranges. Therefore, a piecewise model based on corner frequency is here proposed to simulate the variation of lagged coherency function, that is:

$$\gamma(\omega, d) = \frac{1}{1 + \alpha(\omega_c) d^{q(\omega_c)} \omega^4} \exp[-\beta(\omega_c) d] \quad (11)$$

This model is a rational expression relating frequency  $\omega$  and separation distance  $d$ , in which parameters  $\alpha(\omega_c)$ ,  $q(\omega_c)$ , and  $\beta(\omega_c)$  are related to corner frequency,  $\omega_c$ . This model can be used to solve the analytical solution of correlation coefficients among modes in the response spectrum method under multi-support excitation, which will improve computing efficiency. The parameters of piecewise model for three earthquakes can also be obtained by simulating the lagged coherency function, as are shown in Table 4. It can be seen that a set of parameter can satisfy with the fitting results for two horizontal components. Fig.7 plots the fitting results of Eq. (4) for Parkfield earthquake at 3 frequencies ( $\omega = \pi, 3\pi, 10\pi$ ), in which satisfied fitting results can be obtained in low-frequency and high-frequency ranges. Therefore, these parameters listed in Table 4 can be used to simulate the variation of lagged coherency function under the near-field or far-field earthquake.

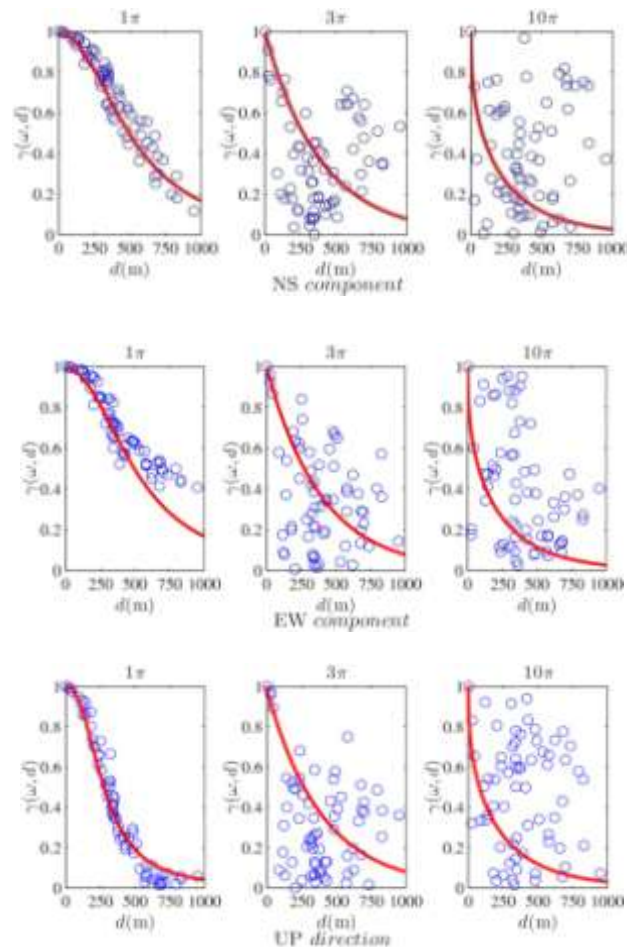


Fig. 7 – Fitting results of piecewise model proposed in this paper for Parkfield earthquake when  $\omega = \pi, 3\pi, 10\pi$



Table 4 – The fitting parameters of piecewise model for three earthquakes

Event	Component	$\alpha(\omega)$	$\beta(\omega)$	$q(\omega)$	$\alpha(\omega)$	$\beta(\omega)$	$q(\omega)$
Wenchuan		$\omega \leq 3\pi$			$\omega > 3\pi$		
	H	$1.15 \times 10^{-8}$	$6.39 \times 10^{-5}$	0.76	$7.78 \times 10^{-12}$	$7.59 \times 10^{-5}$	2.27
	V	$9.16 \times 10^{-12}$	$1.45 \times 10^{-5}$	2.31	$6.78 \times 10^{-12}$	$3.59 \times 10^{-5}$	2.27
San Simeon		$\omega \leq 1.5\pi$			$\omega > 1.5\pi$		
	H	$6.42 \times 10^{-9}$	$2.22 \times 10^{-4}$	2.15	$5.52 \times 10^{-8}$	$2.53 \times 10^{-3}$	0.45
	V	$6.42 \times 10^{-9}$	$2.22 \times 10^{-4}$	2.31	$5.52 \times 10^{-8}$	$2.53 \times 10^{-3}$	0.45
Parkfield		$\omega \leq \pi$			$\omega > \pi$		
	H	$5.06 \times 10^{-9}$	$1.85 \times 10^{-4}$	2.23	$5.52 \times 10^{-8}$	$2.53 \times 10^{-3}$	0.45
	V	$6.42 \times 10^{-9}$	$2.22 \times 10^{-4}$	2.45	$5.52 \times 10^{-8}$	$2.53 \times 10^{-3}$	0.45

## 6. Conclusions

Analysis of the spatial variation of acceleration data of three earthquakes result in following conclusions, definition and new model:

(1) The source-to-site distance affects variation rate of lagged coherency function along with separation distances in low-frequency and high-frequency ranges.

(2) We define “coherency cut-off frequency”, relating to source-to-site distance, to distinguish the variation rates of the variation of lagged coherency function along with separation distances in low-frequency and in high-frequency ranges. The values of coherency cut-off frequency based on different source-to-site distances were determined by analyzing spatial variation of ground motion.

(3) A new piecewise model is presented to simulate the variation of lagged coherency function, with parameters suitable for the conditions of earthquake in the near and far fields. This model relates to the coherency cut-off frequency and can better reflect the changes of the lagged coherency function along with the frequency and separation distance changes.

## 7. Acknowledgements

The financial supports from National Key R & D Program of China (2017YFC0404901) and Natural Science Foundation of China (No. 51878627 and No. 51478440) are much appreciated.

## 8. References

- [1] Hindy, A. and Novak, M.(1980): Response of pipelines to random ground motion. *Journal of Engineering Mechanics*, **106**, 339-360.
- [2] Saxena, V., Deodatis, G. and Shinozuka, M.(2000): Effect of spatial variation of earthquake ground motion on the nonlinear dynamic responses of highway bridges. *Proc of 12th World Conf on Earthquake Engineering*, Auckland, New Zealand.
- [3] Zerva, A.(2009): Spatial variation of seismic ground motions: modeling and engineering applications. *CRC Press*, Taylor and Francis Group: Boca Raton.
- [4] Somerville, P.G., Irikura, K., Graves, R., Sawada, S., Kagawa, T. and Smith, N.(1999): Characterizing crustal earthquake slip models for the prediction of strong ground motion. *Seim. Res. Lett.* **70**(1) 59-80.
- [5] Liao, S, Zerva, A., (2007): Stephenson WR. Seismic spatial coherency at site with irregular subsurface topography. *Proceedings of Sessions of Geo-Denver*, Geotechnical Special Publication **170**, 1-10.



- [6] Feng, Q.M. and Hu, Y.X. (1981): Spatial correlation model of ground motion. *Earthquake Engineering & Engineering Vibration*, **1**, 1-8.
- [7] Luco, J.E. and Wong, H.L. (1986): Response of a rigid foundation to a spatially random ground motion. *Earthquake Engineering & Structural Dynamic*, **14**, 891-908.
- [8] Der Kiureghian, A. (1996): A coherency model for spatially varying ground motions. *Earthquake Engineering & Structural Dynamic*, **25**, 99-111.
- [9] Ding, H.P., Liu, Q.F., Jin, X. and Yuan, Y.F. (2004): A coherency function model of ground motion at base rock corresponding to strike-slip fault. *J. ACTA Seismological Sinica*, **17**, 64-69.
- [10] Hao, H., Oliveira, C.S. and Penzien, J. (1989): Multiple-station ground motion processing and simulation based on SMART-1 array data. *Nuclear Engineering and Design*, **111**(3), 293-310.
- [11] Jankowski, R. and Wilde, K. (2000): A simple method of conditional random field simulation of ground motions for long structures. *Engineering Structures*, **22** (5), 552-561.
- [12] Yu, R.F., Yuan, M.Q. and Yu, Y.X. (2011): Spatial Coherency Function of Seismic Ground Motion Based on UPSAR Records. *Applied Mechanics and Materials*, 90-93, 1586-1592.
- [13] Konakli, K. and Der Kiureghian, A. (2012): Simulation of spatially varying ground motions including incoherence, wave-passage and differential site-response effects. *Earthquake Engineering & Structural Dynamics*, **414**, 95-513.
- [14] Hu, L., Xu, Y.L. and Zheng, Y. (2012): Condition simulation of spatially variable seismic ground motions based on evolutionary spectra. *Earthquake Engineering & Structural Dynamics*, **41**, 2125-2139.
- [15] Fletcher, J.B., Baker, M., Spudich, P., Goldstein, P., Sims, J.D. and Hellweg, M. (1992): The USGS Parkfield, California, dense seismograph array: UPSAR, *Bulletin of the Seismological Society of America*, **00**(0), 1041-1070.
- [16] Boore, D.M. (2001): Effect of baseline correlation on displacement and response spectra for several recordings of the 1999 Chi-Chi, Taiwan, earthquake. *Bulletin of the Seismological Society of America*, **91**, 1199-1211.
- [17] Wang, G.Q., Boore, D.M., Igel, H. and Zhou, X.Y. (2003): Some observation on collocated and closely spaced strong ground motion records of the 1999 Chi-Chi, Taiwan, earthquake. *Bulletin of the Seismological Society of America*, **936**, 74-693.
- [18] Wang, G.Q., Tang, G.Q., Jackson, C.R., Zhou, X.Y. and Lin, Q.L. (2006): Strong ground motions observed at the UPSAR during the 2003 M 6.5 San Simeon and 2004 M 6.0 Parkfield Earthquakes. *Bulletin of the Seismological Society of America*, **96**(4B), 159-182.
- [19] Spudich, P. (1994): Recent seismological insights into the spatial variation of earthquake ground motions. *New Developments in Earthquake Ground Motion Estimation and Implications for Engineering Design Practice*, ATC, 35-1.
- [20] Boissières, H. P., & Vanmarcke, E. H. (1995): Estimation of lags for a seismograph array: wave propagation and composite correlation. *Soil Dynamics and Earthquake Engineering*, **14**(1), 5-22.
- [21] Harichandran, R.S. and Vanmarcke, E.H. (1986): Stochastic variation of earthquake ground motion in space and time. *Journal of Engineering Mechanics*, **112**, 154-174.



[22] Abrahamson, N.A., Schneider, J.F. and Step, J.C. (1991): Empirical spatial coherency functions for applications to soil-structure interaction analyses. *Earthquake Spectra*, **7**, 1-28.